

Communication

Borneol-Modified Chitosan Coating with Antibacterial Properties via Layer-by-Layer Strategy

Zixu Xie, Zhiran Zheng *, Chen Chen, Guofeng Li and Xing Wang * 

Beijing Laboratory of Biomedical Materials, College of Life Science and Technology, Beijing University of Chemical Technology, Beijing 100029, China

* Correspondence: 2020400280@buct.edu.cn (Z.Z.); wangxing@mail.buct.edu.cn (X.W.)

Abstract: Chitosan exhibits remarkable broad-spectrum antibacterial activity, especially in acidic environments. However, its poor solubility in water and significantly decreased antibacterial performance after membrane formation greatly limit its extensive application. To address this issue, glycol chitosan-4-pyridylcarboxaldehydeborneol (GCBP) was synthesized by conjugating glycol chitosan (GC) with 4-pyridylcarboxaldehydeborneol ester (BP) through dynamic Schiff base bonds utilizing a layer-by-layer self-assembly strategy. When bacteria come into contact with the surface, the local acidic microenvironment triggers the cleavage of the Schiff base, resulting in the release of bactericidal BP and GC for combined sterilization. In vitro results demonstrated that the antibacterial properties of GCBP were positively related to the modification layers. The excellent antibacterial performance of the GCBP modification demonstrates not only great potential for clinical urinary catheters but also for broad antibacterial applications in the medical field.

Keywords: chitosan; borneol; stereochemistry; Schiff base; layer-by-layer self-assembly



Citation: Xie, Z.; Zheng, Z.; Chen, C.; Li, G.; Wang, X. Borneol-Modified Chitosan Coating with Antibacterial Properties via Layer-by-Layer Strategy. *Coatings* **2024**, *14*, 381. <https://doi.org/10.3390/coatings14040381>

Academic Editor: Seunghan Oh

Received: 21 February 2024

Revised: 20 March 2024

Accepted: 21 March 2024

Published: 25 March 2024



Copyright: © 2024 by the authors. Licensee MDPI, Basel, Switzerland. This article is an open access article distributed under the terms and conditions of the Creative Commons Attribution (CC BY) license (<https://creativecommons.org/licenses/by/4.0/>).

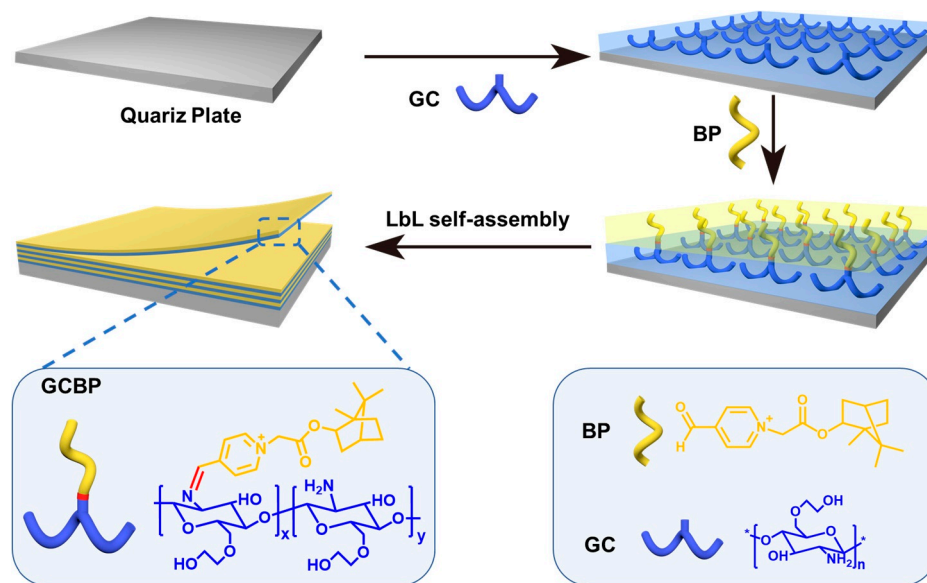
1. Introduction

Chitosan is a polymer obtained through the deacetylation of chitin [1–3] that exhibits both biochemical activity and biocompatibility. After enzymatic degradation in the body, chitosan will break down into a non-toxic substance, giving it advantages for various applications, particularly in the fields of food, biomedicine, biotechnology, and pharmaceuticals [4,5]. Chitosan is well-known for its broad-spectrum antimicrobial properties [6–8], influenced by factors such as deacetylation degree (DD) [9,10], concentration, acetylation pattern (PA), and molecular weight (Mw) [11,12]. Additionally, research has revealed that chitosan has poor solubility in aqueous solutions. Although it demonstrates strong antimicrobial activity in acidic solutions [13], its effectiveness against microbes sharply declines after membrane formation [14], limiting its widespread use.

The layer-by-layer (LbL) self-assembly method has been proven to be a versatile and effective technique for surface modification [15]. The LbL self-assembly process is based on the alternating deposition of charged cations and anionic polyelectrolytes to form a multifunctional polyelectrolyte multilayer film (PEM) on the material's surface [16–18]. PEM films created by LbL deposition can load and release antimicrobial agents on flat surfaces such as silicon, metal, glass, and quartz plates. Subsequent antimicrobial applications have been utilized to modify the surfaces of materials in electronics, machine tools, medical devices, and implants [19–21]. Chitosan is particularly suitable as a polycation in the LbL self-assembly process. The primary amine groups of chitosan can be utilized for LbL self-assembly [22]. Under acidic pH conditions, the amines become positively charged, transforming chitosan into a water-soluble cationic polyelectrolyte form. In addition, the primary amine groups of chitosan can also form covalent bonds with bactericidal components in the form of Schiff base bonds, further enhancing the antibacterial properties of the PEM.

Stereochemical antimicrobial strategies have recently attracted widespread attention [23–25]. Abundant research indicates that polymers containing chiral terpene monomers as antimicrobial components possess inherent antimicrobial adhesion performance, exhibiting excellent resistance to bacterial and fungal adhesion [26–29]. Therefore, modification with borneol, which has specific stereochemical structures, can lead to the antimicrobial performance of chitosan through chiral stereochemistry. However, these modifications typically provide resistance to bacterial adhesion without exhibiting bactericidal properties [26,30]. It is advantageous to introduce a positive charge into the borneol molecules. At the same time, the introduction of a positive charge significantly enhances the bactericidal performance of borneol derivatives.

In general, this study reports a responsive antibacterial strategy against pathogenic microorganisms. Through the esterification process, bromoborneol ester (BBr) is obtained by reacting borneol with bromoacetyl bromide. The BBr then reacts with 4-pyridinecarboxaldehyde to form the BP, which carries a positive charge and an aldehyde group. Subsequently, GCBP was prepared by grafting BP onto GC through a Schiff base. This material conjugates GC with borneol derivatives, resulting in unique stereochemical characteristics using an LbL self-assembly approach (Scheme 1). From the perspective of structure, when a small number of bacteria touches the material's surface, the dynamic covalent bonds of Schiff bases can respond to bacterial stimuli and then release the bactericidal molecules to kill the bacteria. In cases of extensive bacterial growth on the material's surface, the material would completely disintegrate into two parts (GC and BP) and work together to combat bacteria.



Scheme 1. Preparation of GCBP coatings via the LbL self-assembly strategy.

2. Materials and Methods

2.1. Materials

L-Borneol, bromoacetyl bromide, 4-pyridinecarboxaldehyde, and glycol chitosan were purchased from Aladdin Co. (Shanghai, China). Tryptic soy agar (TSA) and tryptic soy broth (TSB) were bought from Beijing Aubergine Co. (Beijing, China). The microbial strains were obtained from the Chinese Industrial Culture Strain Bank.

2.2. Preparation of BBr

To graft borneol molecules onto the long chains of chitosan, BBr, a designed and synthesized intermediate derivative of borneol with an aldehyde group, was obtained through an esterification reaction between borneol and bromoacetyl bromide. Generally, 1 g of L-borneol monomer was added to 15 mL of tetrahydrofuran (THF) under ice bath conditions. After complete dissolution, 700 μ L of pyridine was added as a catalyst. Next,

800 μL of bromoacetyl bromide was diluted with 3.3 mL of dehydrated THF, then it was added dropwise into the borneol mixture using an injection needle. The ice bath condition was removed after 30 min. Finally, an oily product was obtained via washing and filtrating after a 20 h reaction. The BBr powder was obtained after drying in a vacuum oven. ^1H NMR (400 MHz, $\text{DMSO-}d_6$) δ 4.86 (ddd, 1H), 4.21–4.09 (m, 2H), 2.36–2.20 (m, 2H), 1.91 (ddd, 2H), 1.68 (d, 1H), 1.36–1.15 (m, 2H), 0.88 (s, 3H), 0.85 (s, 3H), 0.81 (s, 3H).

2.3. Preparation of BP

0.4 mL of BBr and 0.4 mL of 4-pyridinecarboxaldehyde were dissolved in 2 mL of toluene, respectively. The mixture was degassed under an N_2 atmosphere and kept overnight to form a black precipitate. The product was then washed twice with toluene and dried to obtain a light-yellow solid product (BP). ^1H NMR (400 MHz, $\text{DMSO-}d_6$) δ 10.16 (s, 1H), 9.23 (d, 2H), 8.08 (d, 2H), 6.23 (m, 2H), 4.85 (m, 1H), 2.30 (m, 2H), 1.90 (m, 1H), 1.76–1.65 (m, 2H), 1.38–1.13 (m, 2H), 0.90 (s, 3H), 0.86 (s, 3H), 0.83 (s, 3H).

2.4. Preparation of GCBP-Modified Quartz Plates

Four blank quartz plates were used as the substrate and washed with detergent. After cleaning, the quartz plates were rinsed twice with ultrapure water and then dried with nitrogen. The quartz plates were placed in a glass watch glass and 3 mL of 98% concentrated sulfuric acid was added. Then, 7 mL of 30% hydrogen peroxide (H_2O_2) was added. The solution was mixed by pipetting, soaked for 30 min, and rinsed with ultrapure water several times until the cleaning solution became neutral. The sulfuric acid on the surface of the quartz plate was removed and then dried with nitrogen. To prevent recontamination of the surface, the quartz pieces were immersed in absolute ethanol. The quartz plate was removed from the absolute ethanol and dried with nitrogen. On the surface of the quartz plate, GC and BP were combined via Schiff base reaction using an LbL self-assembly strategy. First, four pieces of quartz plates were placed in a 1 wt% GC aqueous solution, soaked for 2 h, and washed once with water. After being dried, the four quartz plates were immersed in a 1 wt% BP ethanol solution for 2 h, then washed once in ethanol to eliminate excess adsorption. The BP molecules bonded to the main chain of the GC through a Schiff base reaction, achieving the one-layer self-assembly of GCBP on quartz plates. Quartz plates with 2, 3, and 4 layers of GCBP were prepared using the same approach.

2.5. Construction of a GCBP-Modified Urinary Catheter Using LbL Method

A urinary catheter (3 cm in length) was sequentially cleaned with detergent, ultrapure water, concentrated H_2SO_4 , H_2O_2 , and ultrapure water, respectively. The urinary catheter was initially immersed in a 1 wt% GC aqueous solution for 2 h, then washed with water and dried. Subsequently, the urinary catheter was immersed in a 1 wt% BP ethanol solution for 2 h, washed once in ethanol, and dried. The operation was repeated 4 times to obtain 4 layers of a GCBP-modified urinary catheter.

2.6. Testing and Characterization

^1H NMR spectra of monomers and polyesters were obtained using a Bruker AV-500 spectrometer (Saarbrücken, Saarland, Germany) with deuterated dimethyl sulfoxide ($\text{DMSO-}d_6$) as the solvent and tetramethylsilane (TMS) as the internal standard. The UV-vis spectra of monomers and polyesters were obtained using a SHIMADZU UV-3600 spectrometer (Kyoto, Japan). For the dynamic UV-vis test, 20% BBr was added dropwise into 4-pyridinecarbaldehyde and its dynamic UV-vis spectrum was recorded every 5 s. For the UV-vis testing of GCBP-modified quartz plates, 1 to 4 layers of GCBP-modified quartz plates were placed on the optical path of the UV-vis spectrometer for testing.

2.7. Antibacterial Assays

Prison break experiment: A “sandwich structure” was used to observe the inhibition of bacterial growth by the materials [29,31]. 2 μL suspension of pre-prepared *Bacillus subtilis*

(*B. subtilis*) (10^6 CFU/mL) was dropped on the top “TSA island” and then incubated at 37 °C. Changes in the plate were recorded every 24 h using a digital camera.

Plate counting experiment: To quantitatively demonstrate the bactericidal performance of the material, two modes, “1 + 1” and “0 + 1”, were established. For “1 + 1” mode, a GCBP-modified quartz plate was taken as the base. Bacteria ($100 \mu\text{L}$, 3×10^2 CFU/mL) was dropped in the middle, and a GCBP-modified quartz plate was covered on the surface. For “0 + 1” mode, only the GCBP-modified quartz plate was taken as the base, and a blank quartz plate was covered on the surface of the bacteria. Both models were cultured at a constant temperature for 3 h under humid conditions, then sonicated in physiological saline to assess the bactericidal effectiveness of bacteria on GCBP-modified quartz plates.

Co-cultured experiment of a GCBP-modified urinary catheter and bacteria: First, a bacterial suspension with a concentration of 10^8 CFU/mL was diluted 10 times step by step, and then $50 \mu\text{L}$ of the bacterial suspension was placed into a GCBP-modified urinary catheter. After 3 h of contact, they were transferred to a liquid medium for co-culture.

3. Results and Discussion

Firstly, the molecular structure of monomers was analyzed using ^1H NMR. As shown in Figure S2A, each peak in the spectrum can be accurately identified, demonstrating the successful synthesis of BBr. In detail, the peak around 1.0 ppm corresponds to the methyl group ($-\text{CH}_3$) on the cage ring, and the peaks among 1.1–2.4 ppm correspond to several methylene groups ($-\text{CH}_2$) on the cage ring of borneol. The peak at 4.1 ppm corresponds to the methylene group ($-\text{CH}_2$) in bromoacetyl bromide. From the UV-vis spectrum (Figure S2B), only a single peak appears, with the peak intensity corresponding to the peak position of the ester bond at 220 nm, which further confirms the successful synthesis of BBr. From the results in Figure S2C, the peak around 1.0 ppm corresponds to the methyl group ($-\text{CH}_3$) on the cage ring of borneol, and the peaks around 1.1–4.0 ppm correspond to several methylene groups ($-\text{CH}_2$) on the cage ring of borneol. The peak position at 5.2 ppm is slightly shifted from BBr. Peak d corresponds to the methylene group ($-\text{CH}_2$) at 6.1 ppm, which is a newly generated peak after successful synthesis. The peaks at 7.9, 9.4, and 10.3 ppm are the original peaks of tetrapyridinecarbaldehyde. Every peak in the figure can be accurately assigned, demonstrating the successful synthesis of BP.

As shown in Figure S2D, UV-vis spectroscopy of 4-pyridinecarboxaldehyde exhibits two absorption bands. The peak between 240 nm and 260 nm ($\epsilon = 2000$) corresponds to the $\pi \rightarrow \pi^*$ transition, which is similar to benzene. To further demonstrate the success of the synthesis of BP, BBr was added dropwise into 4-pyridinecarbaldehyde, and its dynamic UV-vis spectrum was recorded every 5 s to evaluate the synthesis process. As shown in Figure 1A, the peak intensity of the aldehyde group at 285 nm gradually decreases, while the peak intensity of the newly formed ester bond at 255 nm gradually increases, demonstrating the successful synthesis of the new BP. The UV-vis absorption curve reveals that the peak positions of the BP material are at 225 nm and 255 nm. As depicted in Figure 1B, the peak shape and position of the assembly have not changed. The linear increase in the intensity of the ultraviolet absorption peaks at 225 nm and 255 nm is due to the increased number of modification layers. In addition, the peak of the newly formed Schiff base bond at 305 nm [32] indicates the feasibility of using LbL self-assembly to study GCBP. The above results demonstrate the successful self-assembly process.

The prison break experiments were conducted to validate the antibacterial performance of the materials (Figure 2A). Its procedures involved placing quartz plates on the culture medium and then positioning a small piece of culture medium with a bacterial suspension on the surface of the material. The antibacterial performance of the material is determined by its ability to prevent bacteria from growing outward. As shown in Figure 2B, with the increased number of modified layers, the material’s ability to inhibit bacteria becomes stronger. Bacteria can surpass the limitations of the quartz plate and grow at the fastest rate under a 1-layer GCBP-modified quartz plate. The place surrounding the 4-layer GCBP-modified quartz plate is exceptionally clean, with no visible bacterial growth beyond

the material (Figure 2B,C). It is well-known that antibacterial efficacy is positively related to the number of active materials [33,34]. The antibacterial zone experiment also confirms that with the increase in the number of modification layers, the antibacterial components on the quartz plates increase, thus enhancing the antibacterial activity. Specifically, the 4-layer GCBP-modified quartz plate exhibits the best antibacterial performance (Figure S6). After the inhibition zone experiment, the 4-layer GCBP-modified quartz plate was washed twice with water, dried, and subjected to UV-vis testing to observe changes in signal peaks. The results indicate that after the antibacterial experiment, the overall peak intensity of the 4-layer GCBP-modified quartz plate decreases, suggesting a decrease in the antibacterial component content on the quartz plates, especially the decrease of the C=N peak intensity (Figure S7). This demonstrates that the fracture of C=N leads to the release of antibacterial components, resulting in bactericidal activity. In conclusion, when bacteria touch the surface, GCBP will decompose into GC and BP to kill the bacteria, leading to combined sterilization. These results demonstrate that a GCBP-modified quartz plate will release bactericidal molecules for sterilization by rupturing the Schiff base, and the bactericidal performance of the material will be enhanced with an increased number of modified layers.

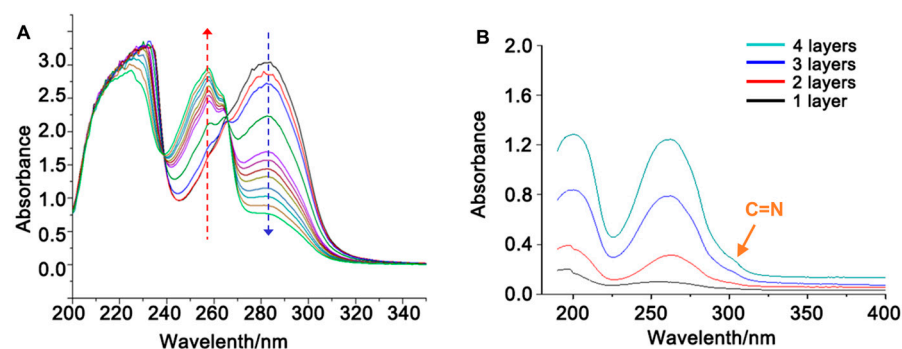


Figure 1. (A) Dynamic UV-vis spectra analysis of the formation of BP; (B) UV-vis spectra of GCBP on a quartz plate after LbL self-assembly.

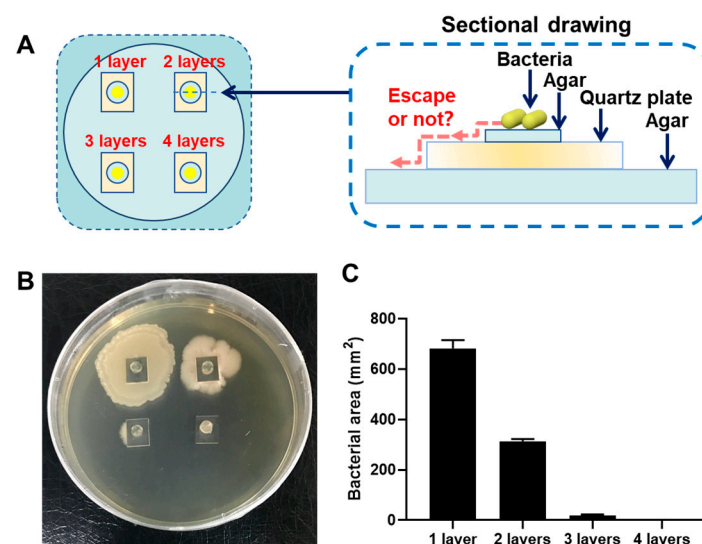


Figure 2. (A) Model of a prison break experiment on a GCBP quartz plate. (B) Prison break experiment of GCBP quartz plates against *B. subtilis*. (C) Statistical histogram of the growth of *B. subtilis*.

To quantitatively demonstrate the bactericidal performance of the GCBP-modified quartz plates, two modes (“0 + 1” and “1 + 1”) were developed (see Figure 3A). The results of the “0 + 1” plate model against *E. coli* are presented in Figure 3B,D. As the number of modified layers of GCBP-modified quartz plates increases, the number of bacteria on the co-incubation plate decreases significantly. Only a few bacteria (7.88% remaining) can be

observed on 4-layer GCBP-modified quartz plates, indicating the excellent bactericidal properties. The results of the “1 + 1” plate count experiment against *E. coli* are presented in Figure 3C,E. When the number of modification layers reaches three or four, the number of bacteria on the plate decreases significantly. Specifically, the count is nearly 0 CFU/mL on 4-layer GCBP-modified quartz plates. Compared to the “0 + 1” mode, the “1 + 1” mode demonstrates a higher antibacterial efficiency. 4-layer modification with GCBP can eliminate almost all bacteria. The sterilization effect is related to the released bactericidal agents by GCBP, and it is clear that the positively charged BP plays a crucial role in this antibacterial process. Typically, the bactericidal performance of positively charged pyridinium is correlated with its carbon chain length [34], requiring a certain carbon chain length to exert antibacterial effects, with optimal antibacterial effects usually achieved at carbon chain lengths of 12–14. If the borneol fragments were replaced with a methyl group (Figure S8), the antibacterial activity of the cation would become very poor. Therefore, the combination of borneol fragments with cations enhances the bactericidal performance of cations, which was confirmed through the MIC test (Table S1).

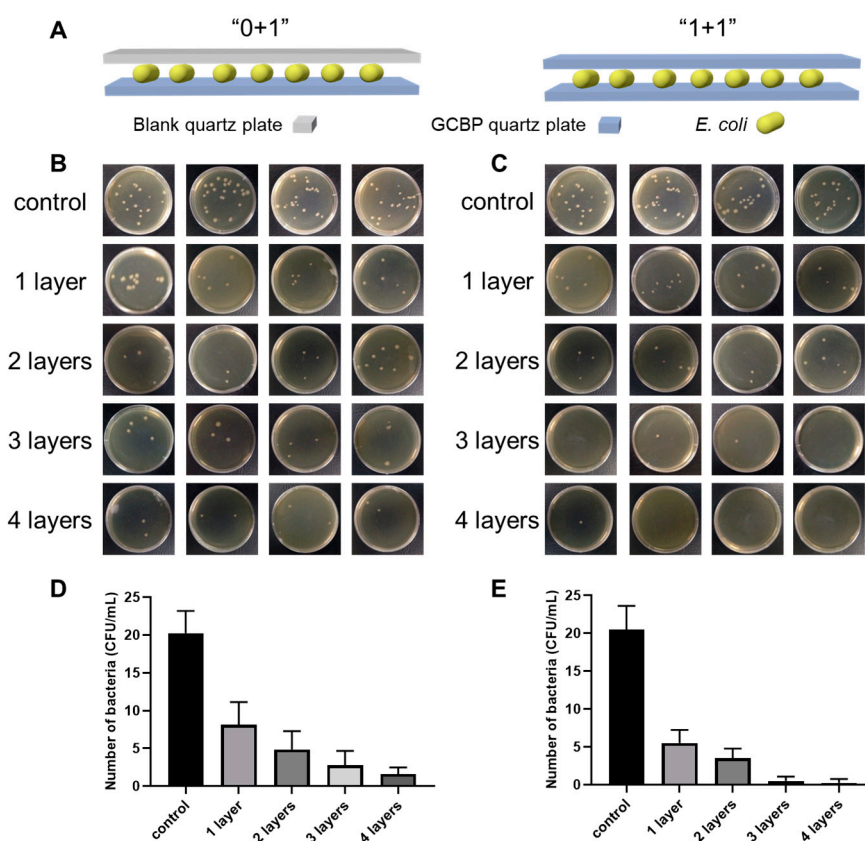


Figure 3. (A) Model diagram of “0 + 1” and “1 + 1” plate count experiments against *E. coli* (100 μ L, 3×10^2 CFU/mL). (B) “0 + 1” plate count results of the GCBP Quartz Plate against *E. coli*. (C) “1 + 1” plate count results of the GCBP Quartz Plate against *E. coli*. (D) The number of bacteria adhering to the GCBP quartz plate of the “0 + 1” plate count experiment against *E. coli*. (E) The number of bacteria adhering to the GCBP quartz plate in the “1 + 1” plate count experiment against *E. coli*.

Finally, the practical antibacterial performance of GCBP was explored on a medical catheter model modified with as-synthesized GCBP. In general, achieving antibacterial effects on medical catheters involves constructing polymer brushes and hydrogel layers on the surfaces or employing methods such as physical adsorption [35]. However, obtaining antibacterial medical catheters through the LBL method can be simpler and more feasible compared to polymer brushes or hydrogel layers. Additionally, it also offers greater stability compared to physical adsorption. Specifically, the 4-layer GCBP-modified urinary catheter

was inoculated with a variety of concentrations of the bacterial solution (from 10^8 CFU/mL to 10^{-1} CFU/mL). After 24 h of cultivation, it was observed that when the concentration of the bacterial solution exceeded 10^3 CFU/mL, the liquid in the test tube became turbid. However, the test tube remained clear and transparent when the concentration was below 10^3 CFU/mL. This distinct effect persisted throughout the entire 120 h incubation period (see Figure 4). Generally, the bacterial number is less than 10^3 CFU/mL in the early stage of infection. Therefore, GCBP modification provides great potential for the clinical application of antibacterial urinary catheters.

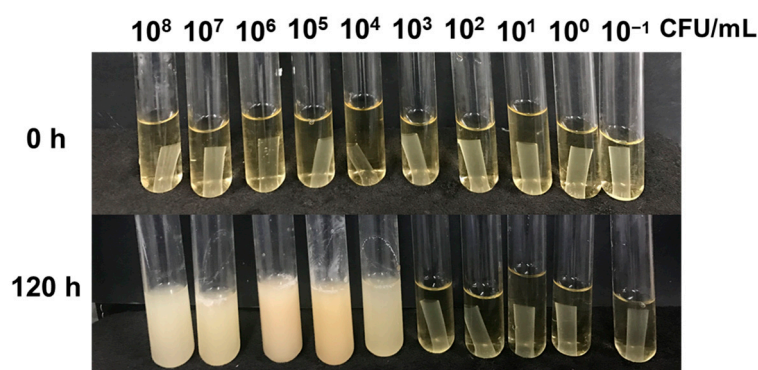


Figure 4. The antibacterial performance of GCBP-modified urethral catheters.

4. Conclusions

In summary, this study developed a novel bactericidal GCBP by grafting BP onto GC through a Schiff base. The introduction of GC, one of the borneol derivatives, endows GCBP with unique stereochemical characteristics. Both the prison break experiments and the plate counting experiments showed that GCBP-modified materials exhibited excellent bactericidal effects for Gram-positive bacteria (*B. subtilis*) and Gram-negative bacteria (*E. coli*). This bactericidal effect was achieved by the breaking of dynamic Schiff base bonds in the acidic microenvironment of bacteria and the release of bactericidal molecules (BP and GC). The positive charge of BP enables it to inhibit the synthesis of the bacterial membrane and ultimately lead to bacterial death [36]. At the same time, GC contributes to anti-bacterial adhesion [37]. In total, the excellent antibacterial performance of GCBP modification provides great potential not only for clinic urinary catheters but also for broad antibacterial applications in the medical field.

Supplementary Materials: The following supporting information can be downloaded at: <https://www.mdpi.com/article/10.3390/coatings14040381/s1>, Figure S1. Procedures for the preparation of glycol chitosan-pyridylcarboxaldehydeborneol (GCBP); Figure S2. (A) ^1H NMR spectra of BBr, (B) UV-vis spectra of BBr, (C) ^1H NMR spectra of BP, and (D) UV-vis spectra of 4-pyridine formaldehyde; Figure S3. Time-dependent UV-vis absorbance changes at 255 nm and 285 nm during the formation of BP. Figure S4. Scanning electron microscope (SEM) images of the 1–4 layer GCBP-modified quartz plates. Figure S5. Prison break experiment of GCBP quartz plates against *E. coli*. Figure S6. Inhibition zone experiment of 1–4 layer GCBP-modified quartz plates against *E. coli*. Figure S7. UV-vis spectra of a 4-layer GCBP-modified quartz plate before (black line) and after (red line) the inhibition zone experiment. Figure S8. ^1H NMR spectra of 4-formyl-1-methylpyridin-1-ium. Table S1. MIC results of GC, 4-Pyridinecarboxaldehyde, BP and 4-formyl-1-methylpyridin-1-ium. References [38,39] are cited in the supplementary materials.

Author Contributions: Formal analysis, Z.X. and Z.Z.; investigation, Z.X. and Z.Z.; data curation, X.W.; writing—original draft preparation, Z.X.; writing—review and editing, Z.Z., C.C., G.L. and X.W.; supervision, X.W.; project administration, X.W.; funding acquisition, X.W. All authors have read and agreed to the published version of the manuscript.

Funding: The authors thank the National Natural Science Foundation of China (52273118, 22275013) for their financial support.

Institutional Review Board Statement: Not applicable.

Informed Consent Statement: Not applicable.

Data Availability Statement: Data are contained within the article and Supplementary Materials.

Acknowledgments: Additionally, we thank Wensheng Xie for revision of the manuscript.

Conflicts of Interest: The authors declare no conflicts of interest.

References

1. Li, J.; Wu, Y.; Zhao, L. Antibacterial activity and mechanism of chitosan with ultra high molecular weight. *Carbohydr. Polym.* **2016**, *148*, 200–205. [[CrossRef](#)] [[PubMed](#)]
2. Sahu, A.; Goswami, P.; Bora, U. Microwave mediated rapid synthesis of chitosan. *J. Mater. Sci. Mater. Med.* **2009**, *20*, 171–175. [[CrossRef](#)] [[PubMed](#)]
3. Di Nardo, T.; Hadad, C.; Nguyen Van Nhien, A.; Moores, A. Synthesis of high molecular weight chitosan from chitin by mechanochemistry and aging. *Green Chem.* **2019**, *21*, 3276–3285. [[CrossRef](#)]
4. Yang, T.-C.; Li, C.-F.; Chou, C.-C. Cell age, suspending medium and metal ion influence the susceptibility of *Escherichia coli* O157:H7 to water-soluble maltose chitosan derivative. *Int. J. Food Microbiol.* **2007**, *113*, 258–262. [[CrossRef](#)] [[PubMed](#)]
5. Li, J.; Zhuang, S. Antibacterial activity of chitosan and its derivatives and their interaction mechanism with bacteria: Current state and perspectives. *Eur. Polym. J.* **2020**, *138*, 109984. [[CrossRef](#)]
6. Jeon, S.J.; Ma, Z.; Kang, M.; Galvão, K.N.; Jeong, K.C. Application of chitosan microparticles for treatment of metritis and in vivo evaluation of broad spectrum antimicrobial activity in cow uteri. *Biomaterials* **2016**, *110*, 71–80. [[CrossRef](#)]
7. Su, Y.; Tian, L.; Yu, M.; Gao, Q.; Wang, D.; Xi, Y.; Yang, P.; Lei, B.; Ma, P.X.; Li, P. Cationic peptidopolysaccharides synthesized by ‘click’ chemistry with enhanced broad-spectrum antimicrobial activities. *Polym. Chem.* **2017**, *8*, 3788–3800. [[CrossRef](#)]
8. Verlee, A.; Mincke, S.; Stevens, C.V. Recent developments in antibacterial and antifungal chitosan and its derivatives. *Carbohydr. Polym.* **2017**, *164*, 268–283. [[CrossRef](#)]
9. Jung, E.J.; Youn, D.K.; Lee, S.H.; No, H.K.; Ha, J.G.; Prinyawiwatkul, W. Antibacterial activity of chitosans with different degrees of deacetylation and viscosities. *Int. J. Food Sci. Technol.* **2010**, *45*, 676–682. [[CrossRef](#)]
10. Chiu, H.-T.; Chen, R.-L.; Wu, P.-Y.; Chiang, T.-Y.; Chen, S.-C. A study on the effects of the degree of deacetylation of chitosan films on physical and antibacterial properties. *Polym.-Plast. Technol. Eng.* **2007**, *46*, 1121–1127. [[CrossRef](#)]
11. Hamdine, M.; Heuzey, M.-C.; Bégin, A. Effect of organic and inorganic acids on concentrated chitosan solutions and gels. *Int. J. Biol. Macromol.* **2005**, *37*, 134–142. [[CrossRef](#)]
12. Yang, R.; Li, H.; Huang, M.; Yang, H.; Li, A. A review on chitosan-based flocculants and their applications in water treatment. *Water Res.* **2016**, *95*, 59–89. [[CrossRef](#)]
13. Zhao, X.; Wu, H.; Guo, B.; Dong, R.; Qiu, Y.; Ma, P.X. Antibacterial anti-oxidant electroactive injectable hydrogel as self-healing wound dressing with hemostasis and adhesiveness for cutaneous wound healing. *Biomaterials* **2017**, *122*, 34–47. [[CrossRef](#)]
14. Foster, L.J.R.; Butt, J. Chitosan films are NOT antimicrobial. *Biotechnol. Lett.* **2011**, *33*, 417–421. [[CrossRef](#)]
15. Zhang, D.; Zhang, X.; Sun, Q.; Zheng, S.; Hao, J.; Wang, Y. Continuous photocatalysis based on layer-by-layer assembly of separation-free tio₂/reduced graphene oxide film catalysts with increased charge transfer and active site. *Eur. J. Inorg. Chem.* **2019**, *5*, 721–729. [[CrossRef](#)]
16. Yan, Y.; Dong, S.; Jiang, H.; Hou, B.; Wang, Z.; Jin, C. Efficient and durable flame-retardant coatings on wood fabricated by chitosan, graphene oxide, and ammonium polyphosphate ternary complexes via a layer-by-layer self-assembly approach. *ACS Omega* **2022**, *7*, 29369–29379. [[CrossRef](#)] [[PubMed](#)]
17. Decher, G. Fuzzy nanoassemblies: Toward layered polymeric multicomposites. *Science* **1997**, *277*, 1232–1237. [[CrossRef](#)]
18. Phuvanartnuruks, V.; McCarthy, T.J. Stepwise polymer surface modification: Chemistry layer-by-layer deposition. *Macromolecules* **1998**, *31*, 1906–1914. [[CrossRef](#)]
19. Dubas, S.T.; Schlenoff, J.B. Swelling and smoothing of polyelectrolyte multilayers by salt. *Langmuir* **2001**, *17*, 7725–7727. [[CrossRef](#)]
20. Dai, J.; Bruening, M.L. Catalytic nanoparticles formed by reduction of metal ions in multilayered polyelectrolyte films. *Nano Lett.* **2002**, *2*, 497–501. [[CrossRef](#)]
21. Zhao, Y.; Hu, J.; Hu, X.; Zhu, F.; Su, J.; Han, J. A novel strategy for fabrication of antistatic and antibacterial fabric via layer-by-layer self-assembly. *Surf. Coat. Technol.* **2023**, *453*, 129143. [[CrossRef](#)]
22. Yi, H.; Wu, L.-Q.; Bentley, W.E.; Ghodssi, R.; Rubloff, G.W.; Culver, J.N.; Payne, G.F. Biofabrication with chitosan. *Biomacromolecules* **2005**, *6*, 2881–2894. [[CrossRef](#)]
23. Luo, L.; Li, G.; Luan, D.; Yuan, Q.; Wei, Y.; Wang, X. Antibacterial adhesion of borneol-based polymer via surface chiral stereochemistry. *ACS Appl. Mater. Interfaces* **2014**, *6*, 19371–19377. [[CrossRef](#)]
24. Hook, A.L.; Chang, C.-Y.; Yang, J.; Luckett, J.; Cockayne, A.; Atkinson, S.; Mei, Y.; Bayston, R.; Irvine, D.J.; Langer, R. Combinatorial discovery of polymers resistant to bacterial attachment. *Nat. Biotechnol.* **2012**, *30*, 868–875. [[CrossRef](#)]
25. Yang, L.; Zhan, C.; Huang, X.; Hong, L.; Fang, L.; Wang, W.; Su, J. Durable antibacterial cotton fabrics based on natural borneol-derived anti-MRSA agents. *Adv. Healthc. Mater.* **2020**, *9*, 2000186. [[CrossRef](#)]

26. Xin, Y.; Zhao, H.; Xu, J.; Xie, Z.; Li, G.; Gan, Z.; Wang, X. Borneol-modified chitosan: Antimicrobial adhesion properties and application in skin flora protection. *Carbohydr. Polym.* **2020**, *228*, 115378. [[CrossRef](#)]
27. Shi, B.; Luan, D.; Wang, S.; Zhao, L.; Tao, L.; Yuan, Q.; Wang, X. Borneol-grafted cellulose for antifungal adhesion and fungal growth inhibition. *RSC Adv.* **2015**, *5*, 51947–51952. [[CrossRef](#)]
28. Chen, C.; Xie, Z.; Zhang, P.; Liu, Y.; Wang, X. Cooperative enhancement of fungal repelling performance by surface photografting of stereochemical bi-molecules. *Colloid Interface Sci. Commun.* **2021**, *40*, 100336. [[CrossRef](#)]
29. Sun, X.; Qian, Z.; Luo, L.; Yuan, Q.; Guo, X.; Tao, L.; Wei, Y.; Wang, X. Antibacterial adhesion of poly (methyl methacrylate) modified by borneol acrylate. *ACS Appl. Mater. Interfaces* **2016**, *8*, 28522–28528. [[CrossRef](#)] [[PubMed](#)]
30. Cheng, Q.; Asha, A.B.; Liu, Y.; Peng, Y.-Y.; Diaz-Dussan, D.; Shi, Z.; Cui, Z.; Narain, R. Antifouling and antibacterial polymer-coated surfaces based on the combined effect of zwitterions and the natural borneol. *ACS Appl. Mater. Interfaces* **2021**, *13*, 9006–9014. [[CrossRef](#)] [[PubMed](#)]
31. Zhang, P.; Chen, X.; Bu, F.; Chen, C.; Huang, L.; Xie, Z.; Li, G.; Wang, X. Dual coordination between stereochemistry and cations endows polyethylene terephthalate fabrics with diversiform antimicrobial abilities for attack and defense. *ACS Appl. Mater. Interfaces* **2023**, *15*, 9926–9939. [[CrossRef](#)] [[PubMed](#)]
32. Kumar, S.; Dutta, J.; Dutta, P.K. Preparation and characterization of N-heterocyclic chitosan derivative based gels for biomedical applications. *Int. J. Biol. Macromol.* **2009**, *45*, 330–337. [[CrossRef](#)]
33. Wang, J.; Sui, M.; Ma, Z.; Li, H.; Yuan, B. Antibacterial performance of polymer quaternary ammonium salt-capped silver nanoparticles on *Bacillus subtilis* in water. *RSC Adv.* **2019**, *9*, 25667–25676. [[CrossRef](#)] [[PubMed](#)]
34. Zhou, Z.; Zhou, S.; Zhang, X.; Zeng, S.; Xu, Y.; Nie, W.; Zhou, Y.; Xu, T.; Chen, P. Quaternary ammonium salts: Insights into synthesis and new directions in antibacterial applications. *Bioconjug. Chem.* **2023**, *34*, 302–325. [[CrossRef](#)] [[PubMed](#)]
35. Liu, L.; Shi, H.; Yu, H.; Yan, S.; Luan, S. The recent advances in surface antibacterial strategies for biomedical catheters. *Biomater. Sci.* **2020**, *8*, 4095–4108. [[CrossRef](#)] [[PubMed](#)]
36. Wang, Y.; Yuan, Q.; Li, M.; Tang, Y. Cationic conjugated microporous polymers coating for dual-modal antimicrobial inactivation with self-sterilization and reusability functions. *Adv. Funct. Mater.* **2023**, *33*, 2213440. [[CrossRef](#)]
37. Chandrasekaran, M.; Kim, K.D.; Chun, S.C. Antibacterial activity of chitosan nanoparticles: A review. *Processes* **2020**, *8*, 1173. [[CrossRef](#)]
38. Mueller, J.H.; Hinton, J. A protein-free medium for primary isolation of the *Gonococcus* and *Me-ningococcus*. *Proc. Soc. Exp. Biol. Med.* **1941**, *48*, 330–333. [[CrossRef](#)]
39. CLSI. *Performance Standards for Antimicrobial Susceptibility Testing*, 25th ed.; Clinical and Laboratory Standards Institute (CLSI): Wayne, PA, USA, 2015; pp. 158–176.

Disclaimer/Publisher’s Note: The statements, opinions and data contained in all publications are solely those of the individual author(s) and contributor(s) and not of MDPI and/or the editor(s). MDPI and/or the editor(s) disclaim responsibility for any injury to people or property resulting from any ideas, methods, instructions or products referred to in the content.